ОБЪЕДИНЕННЫЙ
ИНСТИТУТ
ЯДЕРНЫХ
ИССЛЕДОВАНИЙ

Дубна

E4-98-279

G.Giardina[1], F.Hanappe[2], A.I.Muminov[3], A.K.Nasirov[4]

COMPETITION BETWEEN QUASIFISSION AND FUSION AFTER CAPTURE IN HEAVY-ION COLLISIONS

Submitted to «Известия РАН, серия физическая»

[1]Istituto Nazionale di Fisica Nucleare, Sezione di Catania, and Dipartimento di Fisica dell'Università di Messina; e-mail: qiardina@nucleo.unime.it
[2]Université Libre de Bruxelles, CP 229, B-1050 Bruxelles, Belgium; e-mail: fhanappe@ulb.ac.be
[3]Heavy Ion Physics Department, Institute of Nuclear Physics, 702132 Ulugbek, Tashkent, Uzbekistan
[4]E-mail: nasirov@thsun1.jinr.dubna.su

1998

1 Introduction

In [1], heavy ion fusion reactions were considered as a long dynamical process between the capture of the projectile by the target and formation of the fully equilibrated compound nucleus. As a result an "extra push" energy needed to get compound mononucleus was obtained. But the synthesis of the superheavy elements $Z = 110 - 112$ [2, 3] shows a much smaller "extra push" energy than the one predicted by the macroscopic dynamic model [1]. The peculiarities of the fusion dynamics can be studied by the analysis of the entrance channel effect. The role of entrance channel in the fusion-fission reactions leading to nearly the same compound nucleus was studied in several experiments [4], but the fusion mechanism is not fully understood yet. This fact has a large significance for fusion of massive nuclei where there are large and qualitative differences between capture and fusion processes. The entrance channel effects were also discussed in [5, 6] where authors affirmed that in order to have full understanding of the various data obtained in heavy ion fusion-fission reactions one must include the precompound nucleus dynamics in the analysis of these reactions. Usually, this process is not considered as it should be. The macroscopic models [1, 7] were not suitable for fusion of massive nuclei. The shell structure of the fusing nuclei should be taken into account in calculation.

The study of the entrance channel effects in the dinuclear system (DNS) concept reveals a drastic increase of the quasifission contribution in reactions with the symmetric (or almost symmetric) massive nuclei [8], in the fusion-fission reactions leading to nearly the same compound nucleus [9], and in synthesis of superheavy elements [10, 11, 12]. In the method presented in [8] the capture cross section was calculated in the framework of the optical model and the competition between fusion and quasifission was calculated in a statistical approach. According to this concept the fusion process is considered as a motion in the charge (mass) asymmetry variable, and capture and quasifission are a consequence of the relative motion of nuclei in DNS.

The advantage of the microscopic model application [13, 14, 15] is that it includes the peculiarities of the realistic single-particle states of the projectile and target nuclei. This allows us to calculate the evolution of the single-particle occupation numbers corresponding to the current kinetic energy losses, so the relative and intrinsic motions are considered self-consistently. It was demonstrated that the kinetic energy dissipation in deep-inelastic heavy ion collisions is a gradual process. Its time scale is similar to that of the nucleon exchange process. Notice the model takes into account a dissipation due to a non-exchange process like particle-hole excitations in nuclei. The competition between complete fusion and quasifission of the dinuclear system formed after capture at its further evolution is taken into account by the statistical method as in [8]. An estimation of the capture probability $T_l^{capture}(E, l)$ in a dynamic approach, taking into account the evolution of the relative motion of nuclei and intrinsic motion of their nucleons self-consistently, is an advantage of this paper in comparison with [8]. Therefore, the present model is required to analyse fusion of light nuclei at high energies and of massive nuclei at all energies of collision where quasifission plays a decisive role, decreasing fusion cross section [11, 12].

In Section 2, the general remarks on the considered variables are discussed. Section 3 is devoted to main points of the method. Discussion of the calculated results of the $^{19}F + ^{107}Ag$ and $^{28}Si + ^{98}Mo$ reactions and comparison of theoretical results with experimental data for the $^{40}Ar + ^{nat}Ag$ reaction are made in Section 4. Our conclusions are presented in Section 5.

2 General remarks

In the dinuclear system (DNS) concept the fusion is considered as a transformation of a dinuclear system in a compound nucleus by multinucleon transfer after capture. This means that DNS, formed in the initial stage of collisions, should live for a long enough time to overcome the intrinsic fusion barrier [8] to become mononucleus (compound nucleus). Note this barrier could arise in the way to fusion, particularly in case of fusion of massive nuclei. It is connected with the mass asymmetry degree of freedom. Because of technical difficulties to perform the time dependent microscopic calculations of competition between the fusion and quasifission processes in DNS approach we were obliged to use a statistical way.

The existence of this intrinsic fusion barrier leads to the increase of the quasifission process when dinuclear system formed after capture decays not reaching the compound mononucleus. Notice the fusion of light and intermediate mass nucleus occurs without competition with quasifission at low energies. In this case, the capture cross section can be identified with fusion cross section which is well described in the surface friction model [7] and optical model. The present model gives the same results for fusion and capture cross sections at low energies, since the pocket in nucleus-nucleus potential is usually large enough.

In the formation of massive nuclei the pocket is very shallow and the energy interval leading to the capture of nuclei is narrow. As a result, the colliding system is allowed to trap and capture only at small numbers of partial waves. This limits the interval of excitation energy of dinuclear system after capture and leads to an increase of quasifission which indeed takes place in reactions with massive nuclei. A gradual dissipation of relative kinetic energy comes from the limited value of the friction coefficient [14].

As a result of calculation we find that:

i) a number of partial waves with angular momentum lead to capture (*i.e.*, those partial waves which have been trapped into a potential minimum of the entrance channel; the critical value of angular momentum l_{cr} for a given collision energy can be calculated dynamically);

ii) a value of the excitation energy is available before the complete fusion at given collision energy and impact parameter or orbital angular momentum (the excitation energy also a result of the dynamic calculation);

iii) a beam energy window is favorable to the fusion: the low limit (E_{min}) of this window is defined by the dynamical barrier in the entrance channel before the capture, and the upper limit (E_{max}) appears because friction forces cannot provide an intense loss of the initial kinetic energy in order to trap the dinuclear system into a pocket.

3 Basic formalism

3.1 Capture and fusion cross section in dinuclear system concept

According to the scenario presented in the previous section the evaporation residue cross section is related to the partial fusion cross section $\sigma_l^{fus}(E,l)$, as well as to the probability $W_{sur}(E,l)$ that the compound nucleus survives fission during the de-excitation cascade at the bombarding

energy E:

$$\sigma_{er}(E) = \sum_{l=0}^{\infty} \sigma_l^{fus}(E,l) W_{sur}(E,l), \tag{1}$$

where

$$\sigma_l^{fus}(E) = \frac{\lambda^2}{4\pi}(2l+1) T_l^{capture}(E,l) P_{CN}(E,l). \tag{2}$$

Here λ is a wavelength,

$$T_l^{capture}(E,l) = \begin{cases} 1, & \text{if} \quad l \le l_{cr} \\ 0, & \text{if} \quad l > l_{cr} \end{cases}$$

(where l_{cr} is determined from the equations of motion for the internuclear distance and orbital angular momentum), while the factor $P_{CN}(E,l)$ is used to take into account the decrease of the fusion probability due to dinuclear system break-up competing with fusion. At first this factor was determined in [8]. If DNS has been formed and lives long enough we can calculate the P_{CN} probability of compound nucleus formation using the driving potential of this system.

Knowing the intrinsic fusion barrier B_{fus} versus the mass asymmetry axis (see Fig.1) and the depth of the potential pocket B_{qf} versus the radial distance axis R (see Fig.2) from the driving potential we can calculate the competition between fusion and quasifission. This barrier is determined by the difference between the driving potential maximum in the way to fusion and the point corresponding to the entrance mass asymmetry in the driving potential (Fig.1). The depth of the potential pocket B_{qf} is considered like a quasifission barrier for the given dinuclear system.

The calculation of competition between fusion and quasifission processes can be done according to principles of statistical physics by comparing the level density at the top point in the $U(Z,A;l,R_m)$ driving potential with the level density to the bottom of the pocket of the exit barrier in the $V(Z,A;l,\mathrm{R})$ internuclear potential. The driving potential, playing the main role in a fusion dynamics, was calculated as follows:

$$U(Z,A;l,R_m) = B_1(Z;A) + B_2(Z_P + Z_T - Z; A_P + A_T - A) + V(Z,A;l,R_m) - B_0, \tag{3}$$

where B_1 and B_2 are the binding energies [16, 17] of the nuclei in a dinuclear system, $V(R_m) = V(Z,A,R_m)$ is the minimum value of the nucleus–nucleus interaction potential at the bottom of the pocket; B_0 is the binding energy of the compound nucleus. For the given total charge and mass numbers, $Z_{tot} = Z_1 + Z_2$ and $A_{tot} = A_1 + A_2$, the A/Z ratio of considered fragment was determined from the minimum value of $U(Z,A;l,R_m)$. The method of calculation of $V(R_m)$ is presented in the next section.

The available difference in calculation of the capture and fusion cross sections was required to introduce $P_{CN}(E,l,E^*)$. Analytically this appears as follows:

$$P_{CN}(E,l) = \frac{\psi_{fus}(E^* - B_{fus}(R_m,l))}{\psi_{fus}(E^* - B_{fus}(R_m,l) + \psi_{qf}(E^* - B_{qf}(R_m,l))}, \tag{4}$$

where

$$\psi_K(E^* - B_K(R_m,l)) = \frac{g}{2\sqrt{g_1 g_2}} \frac{\exp\left[2\pi\sqrt{g(E^* - B_K(R_m,l))/6}\right]}{\left[\frac{3}{2} g(E^* - B_K(R_m,l))\right]^{\frac{1}{4}} (E^* - B_K(R_m,l))\sqrt{48}}. \tag{5}$$

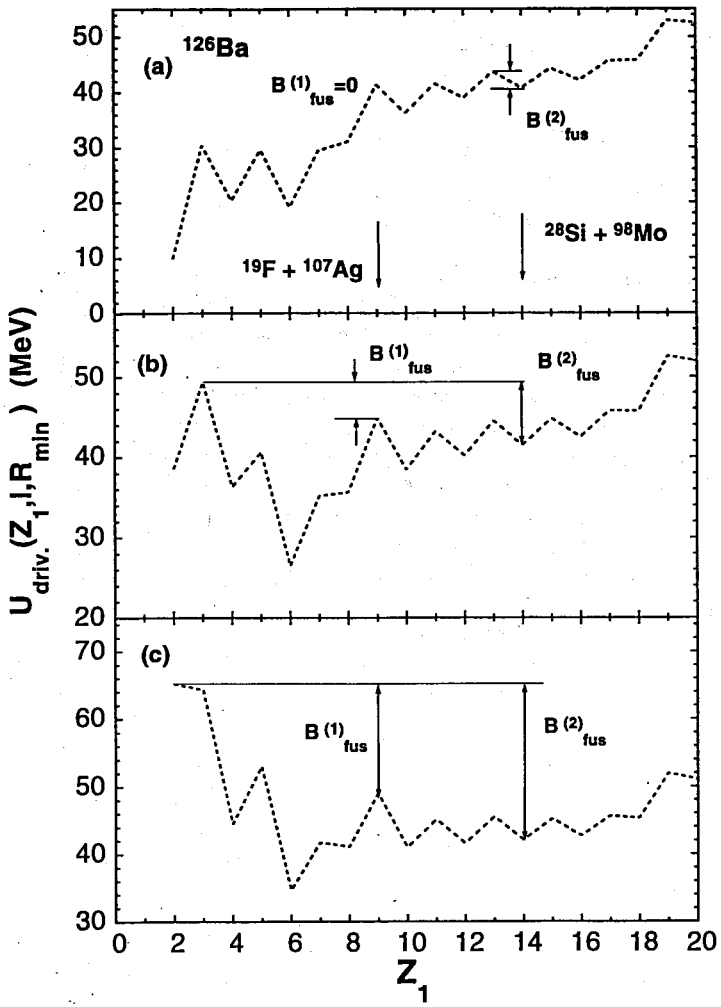

Fig.1. The driving potential (dashed curves) of compound nucleus ^{126}Ba calculated for different values of angular momentum: $l = 0$ (a), $l = 20\hbar$ (b), and $l = 30\hbar$ (c). The different values of the entrance mass asymmetry are shown by arrows ($Z_1 = 9$ and 14). $B^{(1)}_{fus}$ and $B^{(2)}_{fus}$ are intrinsic barriers in the way to fusion for the ^{19}F + ^{107}Ag and ^{28}Si + ^{98}Mo reactions, respectively

Here $E^* = E - V(R_m, l)$ is the excitation energy of the dinuclear system, at the relative distance R_m where an adiabatic nucleus-nucleus potential $V(R_m, l)$ has a minimum; $g = (g_1 + g_2)/2$, and g_1 and g_2 are the level densities of single particle states near the Fermi surface; B_{fus} and B_{qf} are the intrinsic fusion and quasifission barriers, respectively, and they will be discussed in Section 4. The survival probability $W_{sur}(E)$ describes the compound nucleus decay. It is about 1 for the reactions under discussion and therefore it is not considered in this paper.

The factor $T_l^{capture}(E, l)$ is connected with the relative kinetic energy and angular momentum losses which were determined from the equation of motion

$$\mu(\mathbf{R}(t))\ddot{\mathbf{R}} + \gamma_R[\mathbf{R}(t)]\dot{\mathbf{R}}(t) = -\frac{\partial V[\mathbf{R}(t)]}{\partial \mathbf{R}}, \tag{6}$$

$$\frac{dL}{dt} = \gamma_\theta[\mathbf{R}(t)]\left(\dot{\theta}R^2_{eff} - \dot{\theta}_1 R^2_{1eff} - \dot{\theta}_2 R^2_{2eff}\right) \tag{7}$$

where $\mathbf{R}(t)$ is the relative motion coordinate, $\dot{\mathbf{R}}(t)$ is the corresponding velocity; $\dot{\theta}$, $\dot{\theta}_1$ and $\dot{\theta}_2$ are angular velocities of dinuclear system and its fragments, respectively;

$$R_{eff} = \frac{R + R_1 + R_2}{2}, R_{1(2)eff} = \frac{R_{1(2)}}{R_1 + R_2}R.$$

The friction coefficients γ_R and γ_θ, a change of the nucleus-nucleus potential during interaction of nuclei,

$$V[\mathbf{R}(t)] = V_0[\mathbf{R}(t)] + \delta\hat{V}(\mathbf{R}), \tag{8}$$

and the dynamic contribution $\delta\mu(\mathbf{R})$ to the reduced mass

$$\mu(\mathbf{R}) = mA_TA_P/(A_T + A_P) + \delta\mu(\mathbf{R}) \tag{9}$$

are calculated from the estimation of the coupling term between relative motion of nuclei and intrinsic excitation of nucleons in them [14]. The explicit expressions of these quantities induced by dynamics of heavy ion collisions will be presented in Section 3.3.

3.2 Hamiltonian of collision

In this model the capture of colliding nuclei at the initial stage is described by the total Hamiltonian of a dinuclear system written in the form

$$\hat{H} = \hat{H}_{rel}(\mathbf{R};\mathbf{P}) + \hat{H}_{in}(\xi) + \delta\hat{V}(\mathbf{R},\xi), \tag{10}$$

where the Hamiltonian of a relative motion,

$$\hat{H}_{rel}(\mathbf{R};\mathbf{P}) = \frac{\hat{\mathbf{P}}^2}{2\mu} + \hat{\mathcal{V}}(\hat{\mathbf{R}}), \tag{11}$$

consists of the kinetic energy operator and the nucleus-nucleus interaction potential $\hat{\mathcal{V}}(\hat{\mathbf{R}})$. Here, $\hat{\mathbf{R}}$ is the relative distance between the centers of mass of the fragments, $\hat{\mathbf{P}}$ is the conjugate momentum, ξ is a set of relevant intrinsic variables. The last two terms in (10) describe the internal motion of nuclei and the coupling between the relative and internal motions. The effect of inelastic excitations is explored in Section 3.3.

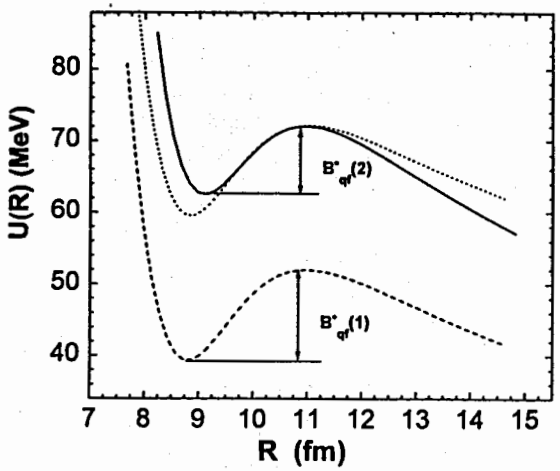

Fig.2. The nucleus-nucleus potential $U(R)$ calculated for the ^{28}Si + ^{98}Mo (solid curve) and ^{19}F +^{107}Ag (dashed curve) reactions as a function of internuclear distance. For an easier comparison of two pockets (in width and depth) the dashed curve is shifted (dotted curve) up to overlapping with the solid curve. $B^{(1)}_{qf}$ and $B^{(2)}_{qf}$ are quasifission barriers for the corresponding reactions

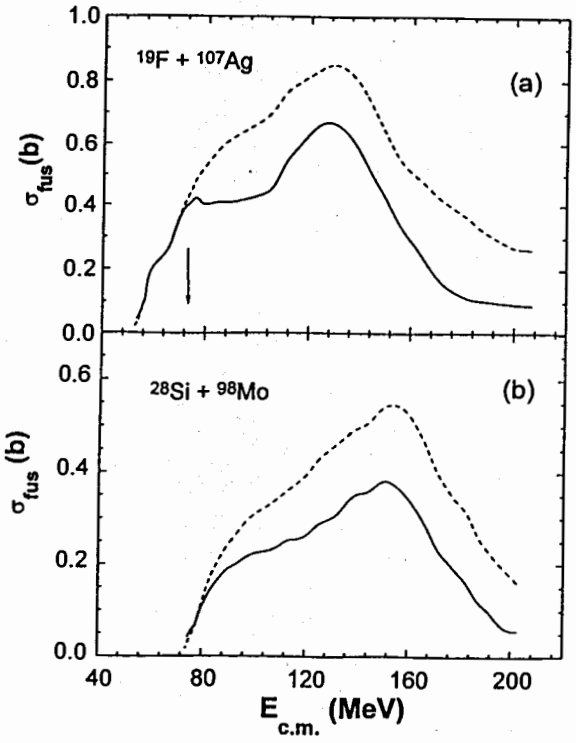

Fig.3. The fusion cross sections σ_{fus} against the collision energy in center-of-mass system, calculated in the present model (solid curve) and the same (dashed curve), but obtained when one assumes P_{CN}=1 in formula (2): for the ^{19}F +^{107}Ag (a) and ^{28}Si + ^{98}Mo reactions (b)

The dynamics of capture is sensitive to nucleus-nucleus potential

$$V(\mathbf{R}) = V_C(\mathbf{R}) + V_{nucl}(\mathbf{R}) + V_{rot}(\mathbf{R}), \tag{12}$$

where $V_C(\mathbf{R}), V_{nucl}(\mathbf{R})$, and $V_{rot}(\mathbf{R})$ are the Coulomb, nuclear and rotational potentials, respectively. The nuclear shape is an important ingredient to calculate the Coulomb and nuclear interaction between colliding nuclei. Thus, the Coulomb interaction of quadrupole deformed nuclei was calculated according to the expressions from [18]:

$$\begin{aligned} V_C(R) &= \frac{Z_1 Z_2}{R} e^2 \\ &+ \frac{Z_1 Z_2}{R^3} e^2 \left\{ \left(\frac{9}{20\pi}\right)^{1/2} \sum_{i=1}^{2} R_{0i}^2 \beta_{2i} \mathcal{P}_2(\cos\alpha_i) + \frac{3}{7\pi} \sum_{i=1}^{2} R_{0i}^2 \left[\beta_{2i} \mathcal{P}_2(\cos\alpha_i)\right]^2 \right\}, \end{aligned} \tag{13}$$

where Z_i, R_{0i}, and α_i are the atomic number, the effective half density radius, and an angle between the line connecting mass centers of nuclei and the axial symmetry axis of the fragment $i (i = 1, 2)$, respectively; $\mathcal{P}_2(\cos\alpha)$ is the second term of the Legendre polynom. The nuclear part of nucleus-nucleus potential is calculated using the folding procedure between the effective nucleon-nucleon forces $f_{eff}[\rho(x)]$ suggested by Migdal [19] and the nucleon density of projectile- and target-nucleus

$$V_{nucl}(\mathbf{R}) = \int \rho_1^{(0)}(\mathbf{r} - \mathbf{R}_1) f_{eff}[\rho(r)] \rho_2^{(0)}(\mathbf{r} - \mathbf{R}_2) d^3\mathbf{r} \tag{14}$$

where $\rho = \rho_1^{(0)} + \rho_2^{(0)}$; $\mathbf{R}_i$ $(i = 1, 2)$ is the position of the center of mass of the fragment i. The nucleon densities are assumed as a Fermi distribution

$$\rho_i^{(0)}(\mathbf{r}, \mathbf{R}_i(t), \alpha_i, \beta_2^{(i)}) = \left\{ 1 + \exp\left[\frac{|\mathbf{r} - \mathbf{R}_i(t)| - R_{0i}(1 + \beta_2^{(i)} Y_{20}(\alpha_i))}{a} \right] \right\}^{-1}, \tag{15}$$

where $\beta_2^{(i)}$ and α_i are their quadrupole deformation parameters and the axis orientation of the axial symmetry, respectively. Taking into account the deformation and orientation of nuclei allows us to consider nuclear collisions at so-called subbarrier energies. The explicit expression for the folding procedure with the nucleon density of the arbitrary–oriented colliding nuclei is presented in Appendix A.

The orientation influences the geometrical cross section of the collision not so much as the value of l_{cr} determining the reaction cross section. In collisions with tip-tip orientation the size of the pocket in the nucleus-nucleus potential is larger (deeper and wider) than in case of side-side orientation.

The additional deformation of one nucleus in the field of another partner is taken into account as an excitation of 2^+ collective states which are easily populated at the near Coulomb barrier energies. The strong coupling to excited states leads to a set of Coulomb barriers of different heights and "weights" [20-23]. In our approach, relative motion was treated by including excitation of collective first 2^+ state of nuclei. The quadrupole deformation parameter β_2 was obtained from the experimental $B(E2)$ values [24]. It was assumed that these states are easily populated at near barrier energies and are damped during interaction: the relaxation time of shape degrees of freedom is larger than one of relative motion. The shape of the nuclei of dinuclear systems changes by the evolution of the mass asymmetry degrees of freedom. In

order to calculate the potential energy surface as a function of charge number, we use the $\beta_2^{(2+)}$ deformation parameter from the data in [24]. The atomic number was fixed from the minimum of the potential energy surface, the latter being considered as a function of $A_1 = A_{tot} - A_2$ at every intermediate charge number of the DNS nuclei.

The rotational potential is calculated in the usual way:

$$V_{rot}(\mathbf{R}) = \hbar^2 \frac{l(l+1)}{2\mu R^2}. \tag{16}$$

Taking the deformation of colliding nuclei into account means using the nucleus-nucleus potential depending on the mutual orientations of symmetry axis of the colliding nuclei. As a result the value and position of the entrance barrier and the pocket size in potential are dependent on the relative orientation of the axial symmetry axes of colliding nuclei. The final fusion cross section is obtained after averaging $\sigma_l(E)$ over all orientations. These effects are very important to interpret the results obtained at subbarrier energies for all nuclei. Particularly, using the dependence of the collision orientation in calculation, we reproduced the beam energy values at which the excitation functions in the synthesis of the $Z = 110, 111$ superheavy elements were experimentally obtained [25].

3.3 Intrinsic energy and kinetic coefficients

The inelastic excitation of nuclei is inherent in the initial stage of heavy ion collisions. Damping of the relative kinetic energy and angular momentum is obtained by a self-consistent solution of the equations of the intrinsic degrees of freedom and relative distance [13, 14]. Friction coefficients of relative motion and the dynamical change of the nucleus-nucleus interaction are due to the nucleon exchange and particle-hole excitation in the fragments of a dinuclear system.

To consider the interaction dynamics between relative motion and nuclear intrinsic motion the last two terms in (10) are obtained in the second quantized form

$$\hat{\mathcal{H}}(\mathbf{R}(t),\xi) = \hat{H}_{in}(\xi) + \delta\hat{V}(\mathbf{R},\xi) = \sum_P \varepsilon_P \mathrm{a}_P^\dagger \mathrm{a}_P + \sum_T \varepsilon_T \mathrm{a}_T^\dagger \mathrm{a}_T + \sum_{i,i'} V_{ii'}(\mathbf{R}(t)) \mathrm{a}_i^\dagger \mathrm{a}_{i'} + h_{res}, \tag{17}$$

where

$$\sum_{i,i'} V_{ii'}(\mathbf{R}(t)) \mathrm{a}_i^\dagger \mathrm{a}_{i'} = \sum_{P,P'} \Lambda_{PP'}^{(T)}(\mathbf{R}(t)) \mathrm{a}_P^\dagger \mathrm{a}_{P'} + \sum_{T,T'} \Lambda_{TT'}^{(P)}(\mathbf{R}(t)) \mathrm{a}_T^\dagger \mathrm{a}_{T'} + \sum_{T,P} \mathrm{g}_{PT}(\mathbf{R}(t)) (\mathrm{a}_P^\dagger \mathrm{a}_T + \mathrm{h.c.}). \tag{18}$$

Here $\varepsilon_P(T)$ are the single-particle energies of nonperturbed states in the projectile (target) nucleus; $\Lambda_{PP'}^{(T)}$ ($\Lambda_{TT'}^{(P)}$) are the nondiagonal matrix elements generating the particle-hole transitions in the projectile (target) nucleus and the matrix elements g_{PT} which are responsible for the nucleon exchange between reaction partners. These matrix elements are calculated using the approach proposed in [28, 29]. Since an explicit allowance for the residual interaction h_{res} is very complicated it is customary to take into account a two–particle collision term in the linearized form (τ approximation) [13, 26, 27] which is discussed later.

It is clear that the coupling term $\delta\hat{V}(\mathbf{R},\xi)$ leads to dissipation of the kinetic energy into the energy of internal nucleon motion. The coupling between the intrinsic nuclear degrees of

freedom and the collective variable $\mathbf{R}$ is introduced by the $\mathbf{R}$ dependence of the transition matrix elements over the single-particle potentials

$$V_{ik}(\mathbf{R}(t)) = \langle i|\hat{V}_P(\mathbf{r}_i - \mathbf{R}(t)) + \hat{V}_T(\mathbf{r}_i)|k\rangle \tag{19}$$

of the projectile-like and target-like components of the dinuclear system. The trajectory calculation shows that the relative distance $\mathbf{R}(t)$ between the centers of the interacting nuclei could not be less than the sum of their radii. Therefore the tail of the partner single-particle potentials can be considered as a perturbation disturbing the asymptotic single-particle wave functions $|i\rangle, |k\rangle$ and their energies ε_i.

Using the Hamiltonian (17) and applying the formalism of the linear response theory we get the following expression for the friction tensor:

$$\gamma_{kj}[\mathbf{R}(t)] = \sum_{i,i'} \frac{\partial V_{ii'}[\mathbf{R}(t)]}{\partial R_k} \frac{\partial V_{ii'}[\mathbf{R}(t)]}{\partial R_j} B_{ii'}^{(1)}(t), \tag{20}$$

where

$$B_{ik}^{(n)}(t) = \frac{2}{\hbar}\int_0^t dt'(t-t')^n \exp\left(\frac{t'-t}{\tau_{ik}}\right) \sin\left[\omega_{ik}(\mathbf{R}(t'))(t-t')\right] \times [\tilde{n}_k(t') - \tilde{n}_i(t')], \tag{21}$$

$$\hbar\omega_{ik} = \epsilon_i + \Lambda_{ii} - \epsilon_k - \Lambda_{kk}. \tag{22}$$

Here $\tau_{ij} = \tau_i\tau_k/(\tau_i+\tau_k)$; τ_i is the parameter describing the damping of the single-particle motion. The expression for τ_i is derived in the theory of quantum liquids [27] using the effective nucleon-nucleon forces from [19] (see Appendix B). The physical meaning of τ is explained below. This parameter approximately describes the effect of the residual interaction in $\mathcal{H}$.

The dynamical contribution $\delta V[\mathbf{R}(t)]$ to the nucleus–nucleus potential is calculated using the expression

$$\delta V[\mathbf{R}(t)] = \sum_{i,i'} \frac{\partial V_{ii'}[\mathbf{R}(t)]}{\partial R} \frac{\partial V_{ii'}[\mathbf{R}(t)]}{\partial R} B_{ii'}^{(0)}(t), \tag{23}$$

where $B_{ii'}^{(0)}(t)$ is given by Eq. (21).

The third important ingredient of Eq. (6) is the reduced mass $\mu[\mathbf{R}(t)]$ which is calculated using the expression

$$\mu(\mathbf{R}) = mA_TA_P/(A_T + A_P) + \delta\mu(\mathbf{R}), \tag{24}$$

where $\delta\mu(\mathbf{R})$ is the dynamic contribution to the reduced mass. This dynamic correction is calculated using the expression of the same type as found in the linear response theory:

$$\delta\mu[\mathbf{R}(t)] = \sum_{i,i'} \frac{\partial V_{ii'}[\mathbf{R}(t)]}{\partial R} \frac{\partial V_{ii'}[\mathbf{R}(t)]}{\partial R} B_{ii'}^{(2)}(t), \tag{25}$$

where $B_{ii'}^{(2)}(t)$ is given by Eq. (21).

Since Eq. (6) is applied only to describe the initial stage of a colliding nucleus interaction (capture probability) we suppose that this approximation is quite satisfactory.

To calculate all these quantities it is necessary to know the occupation numbers of the single-particle states. Since the excitation energy of the interacting nuclei changes significantly

during the collision, it is necessary to take into account the time dependence of the occupation numbers. This has been made by a numerical solution of the corresponding equations, which has been derived in [15, 30] starting from the von Neumann type equation for a density matrix and doing some approximations. The width of single-particle excitations due to a two-particle collision was taken into account using the linearized form (τ approximation) of the collision integral [13, 26, 27]. Then the equation for the occupation numbers of the single-particle states takes the form

$$i\hbar\frac{\partial\hat{\tilde{n}}(t)}{\partial t} = [\hat{\mathcal{H}}(\mathbf{R}(t)), \hat{\tilde{n}}(t)] - \frac{i\hbar}{\tau}[\hat{\tilde{n}}(t) - \hat{\tilde{n}}^{eq}(\mathbf{R}(t))], \qquad (26)$$

where $\tau = \{\tau_i\}$, $\tilde{n}^{eq}(\mathbf{R}(t))$ is the local quasi-equilibrium distribution function of nucleons over the single-particle state, *i.e.* a Fermi distribution with the temperature $\Theta(t)$ corresponding to the excitation energy at the internuclear distance $\mathbf{R}(t)$. In derivation of the final equation for the diagonal matrix elements of $\tilde{n}(t)$, which are the occupation numbers of the single-particle states $n_i(t)$, it was also assumed that the phases of the nondiagonal matrix elements of $\tilde{n}(t)$ are chaotic.

The trajectory for the given orbital angular momentum at the beam energy E_{lab} was calculated by the way of numerical solution of equations (6) and (26) self-consistently using the time step Δt. The latter was chosen to satisfy the smallness condition of perturbating part in the equation of occupation numbers (26).

4 Results and discussion

The incident projectile energy, atomic masses, and charges of the colliding nuclei are the initial information used in the calculations. The single-particle potentials of the colliding nuclei are taken in the Woods-Saxon form with the parameters r_0=1.15 fm and a = 0.54 fm. The characteristic time parameter Δt (introduced in Section 3.3 in order to solve Eq. (26)) is taken to be equal to $0.8{\cdot}10^{-22}$ s.

The description of the relative motion depends on the nucleus-nucleus interaction potential, which is determined by a double folding of the effective nuclear and Coulomb interactions of the nucleons with the nuclear densities of the interacting nuclei. Due to nucleon exchange and particle-hole excitations the nuclear densities of the colliding nuclei evolve during the reaction and the nucleus-nucleus potential correspondingly changes [13, 15]. This effect is included in our calculations. In contrast to the classical model, assuming the idea of fast kinetic energy losses and thermalization of the excitation energy at the beginning of the reaction, our model and results support the idea of a gradual kinetic energy dissipation. This conclusion is in line with the results of the analysis of the very heavy ion collision mechanism [31]. The kinetic energy of the relative motion is found to be dissipated as nucleons are exchanged, indicating that the time scales of both processes are similar.

In Fig.3, the fusion cross sections (σ_{fus}) calculated by the presented model (solid curve) and the cross section (dashed curve) obtained when one assumes P_{CN}=1 in formula (2) for the ^{19}F $+^{107}$Ag (a) and ^{28}Si + ^{98}Mo (b) reactions are shown. It is clear that the dashed curve describes the capture cross section (σ_{cap}), *i.e.* where there is no quasifission. Therefore, in this case the capture and fusion cross sections are exactly alike.

The first common feature is *i*) an energy window for the capture and fusion processes. The low limit (E_{min}) of this window is determined by the dynamic barrier in the entrance channel before capture; the upper limit (E_{max}) comes from the incomplete dissipation of the relative kinetic energy. When the beam energy is larger than E_{max}, a binary transfer reaction would be observed. In the presented dynamic model, the values of E_{min} and E_{max} (which define the size of the energy window) are determined by both the intense dissipative forces and the size of the pocket in the $U(R)$ nucleus-nucleus potential (Fig. 2). At beam energies larger than E_{max}, the limited magnitude of friction forces could not provide the sufficiently intense loss of initial kinetic energy to trap the dinuclear system into a pocket. This is an important point in reactions with massive nuclei, where $U(R)$ usually has a small pocket.

The second common feature is *ii)* a deviation of the fusion and capture cross sections starting from the definite excitation energy E^*_{dev} (its value is indicated by an arrow in Fig. 1 for each reaction in respect to the threshold of capture) (see Figs. 3a and 3b). The difference between solid and dashed curves is due to the inclusion of the quasifission process. The solid curve represents the complete fusion of DNS in competition with quasifission. For the ^{19}F $+^{107}$Ag (Fig. 3a) and ^{28}Si + ^{98}Mo (Fig. 3b) reactions there is a quantitative difference in the interval of the excitation energy in which the capture and fusion cross sections are coincident. This is connected with the difference in the corresponding ratios of the quasifission B_{qf} (Fig. 2) and intrinsic fusion B_{fus} barriers of these reactions (Fig. 1). One can see that there is not an intrinsic fusion barrier ($B^{(1)}_{fus} = 0$) for the ^{19}F $+^{107}$Ag reaction while it is about 3 MeV for the ^{28}Si + ^{98}Mo reaction at small values of the orbital angular momentum (Fig. 1a). At the same time the first reaction has a larger quasifission barrier than the second one ($B^{(1)}_{qf} > B^{(2)}_{qf}$) (Fig. 2). As a result of these peculiarities of the entrance channel we obtain a larger difference between the fusion and capture cross sections in the ^{28}Si + ^{98}Mo (Fig. 3b) reaction than in the ^{19}F $+^{107}$Ag (Fig. 3a) one. Another consequence of the entrance channel effect is a difference in absolute value of the capture cross sections (Fig.4a), and of the fusion cross sections in Fig. 4b of the above-mentioned reactions. So, the first peculiarity of the entrance channel is the pocket size of the nucleus-nucleus interaction potential, which is different for these reactions (Fig. 2). In the case of the larger pocket (dashed curve) more partial waves contribute to the capture cross section than in the other case (solid curve). From Fig. 4b it is seen that σ_{fus} is larger for the ^{19}F + ^{107}Ag reaction in comparison with the ^{28}Si + ^{98}Mo one, at the same excitation energy (apart from a little interval at the high energy tail), although both reactions give the same compound nucleus but with a different angular momentum distribution (see Fig. 5).

The second peculiarity of the entrance channel is different B_{fus} intrinsic fusion barriers for various initial values of the mass (charge) asymmetry. In case of complete fusion, both of these reactions lead to the same compound nucleus ^{126}Ba and they are driven by the same driving potential, calculated using (3). The entrance point is defined by the charge and the atomic number of the projectile (the arrows in Fig. 1a). While there is no fusion barrier at small angular momenta for the ^{19}F + ^{107}Ag reaction (more asymmetric than another one), there is a finite value of B_{fus} for the ^{28}Si + ^{98}Mo reaction (more symmetric) (see Fig.1a). In this case the system has to overcome B_{fus} to fuse. In addition, the quasifission barrier for the first reaction is larger than that for the second one (see Fig. 2, $B^{(1)}_{qf} > B^{(2)}_{qf}$). This means that the second reaction suffers more quasifission as compared with the first one. As a result, also for this reason, we obtained smaller fusion cross sections for the ^{28}Si + ^{98}Mo reaction in comparison with ^{19}F + ^{107}Ag.

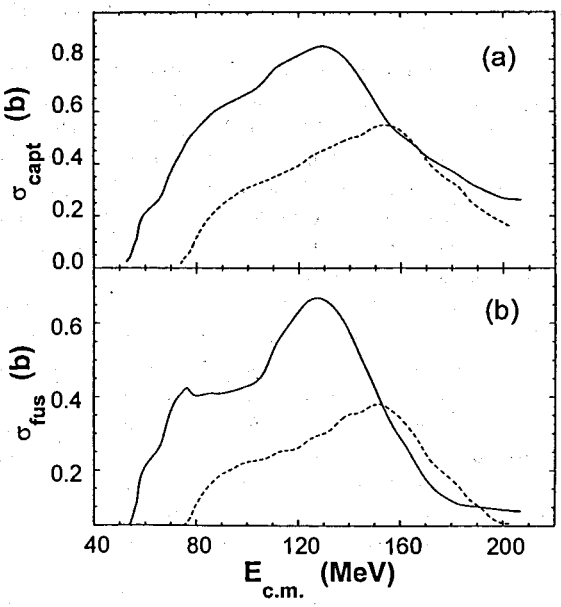

Fig. 4. Comparison between the capture (a) cross sections calculated for the ^{28}Si + ^{98}Mo (dashed curve) and ^{19}F +^{107}Ag (solid curve) reactions, and between the fusion (b) cross sections calculated for the same reactions

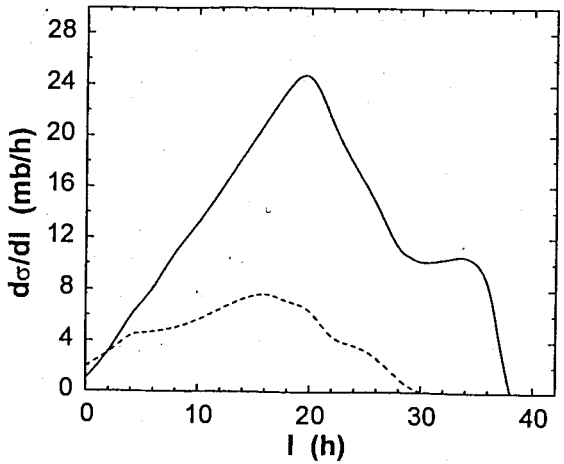

Fig.5. The spin distribution calculated for the ^{19}F + ^{107}Ag (solid curve) and ^{28}Si + ^{98}Mo (dashed curve) reactions

The spin distributions for these reactions are shown in Fig. 5. The effect of the entrance channel leads to larger values of the cross sections for the ^{19}F + ^{107}Ag reaction because of larger values of the spin distribution. It is clear that the deeper and wider potential pocket allows one to include more contributions of partial waves. Only the presence of the competition between quasifission and complete fusion leads to the large difference in the absolute value of $\sigma_l = d\sigma_{fus}/dl$ and its extension on the angular momentum axis.

In order to show the role played by quasifission in reactions with massive nuclei, we compare (see Fig. 6) the calculated capture (dashed curve), fusion (solid curve), evaporation residue (dotted curve and solid circles) cross sections to the experimental data of the evaporation cross section (solid symbols) and to the estimations deduced from the experiments of the fusion cross sections (stars and open symbols) for the ^{40}Ar + ^{nat}Ag reaction. The experimental data were obtained from [32-37] where the fusion process and/or the mechanism of light charged particle emission were studied.

Our fusion calculation (and the evaporation residue calculations too) are in good agreement with the measured evaporation residue production at beam energies up to E_{lab}=337 MeV, apart from a larger deviation registered for the measurement at 288 MeV. This result is in agreement with our estimation for which the fission contribution (dotted-dashed curve in Fig. 6) is small in comparison with the evaporation residue production (dotted curve) (therefore W_{sur} is about 1), while when the quasifission starts (at about 160 MeV of the beam energy) it becomes comparable or larger than the fusion increasing the energy. The smallness of fission contribution (see dotted-dashed curve in Fig. 6) confirms that the decrease of fusion and evaporation cross section, by increasing the beam energy, is caused mainly by the entrance channel effects as the capture and quasifission cross sections. As a result, the evaporation residue measurements for the ^{40}Ar + ^{nat}Ag reaction are comparable with the fusion cross sections obtained in our model.

The main goal of the present paper is to clarify the evident difference between the fusion cross section extracted from the experimental data (of evaporation residue nuclei and/or light charged particles emission spectra) and our calculated fusion cross section. According to our model the dinuclear system, formed after the capture of colliding nuclei, survives quasifission in order to be transformed into a compound nucleus. This stage is fusion and, therefore, the fusion process is a mechanism in competition with the quasifission. Then, if mononucleus survives fission we obtain, as a product, evaporation residue nuclei. In this case the quasifission takes place along the way between the dinuclear system (capture) and the compound nucleus formation (fusion).

Other authors, particularly the authors of Refs.[32-37], consider the quasifission as a process that occurs before the compound nucleus reaches the configuration of the saddle point. Therefore, both this process (fast fission), as a kind of fission, and standard fission are considered in competition with the light particle emission (that leads to evaporation residue formation). In this case, the quasifission fragments are some of the products of the compound nucleus decay and the fusion cross section is the sum of the evaporation residue production and fission fragment formation cross sections. Since a large part of fission fragments coming from the fast fission (which are not easily distinguishable from our quasifission products)and the ones coming from the standard fission overlap, the fusion cross section extracted from the experimental data of the light charged particle emission spectra is overestimated. Therefore, from our point of

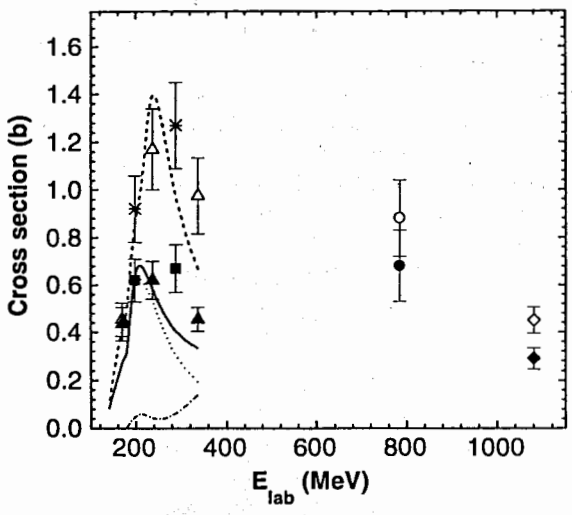

Fig. 6. The experimental data of the fusion (stars and open symbols) and evaporation residue (solid symbols) cross sections from [32-36] for the ^{40}Ar + ^{nat}Ag reaction are compared with the capture (dashed curve), fusion (solid curve) and evaporation residue (solid circles and dotted curve) cross sections calculated in the present work, while the dotted-dashed curve represents the fission contribution. The triangles and stars are the experimental data of Refs. [32,33], the squares are the experimental data of Ref. [34], the circles are the data given in [35], and the diamonds are the data given in [36]

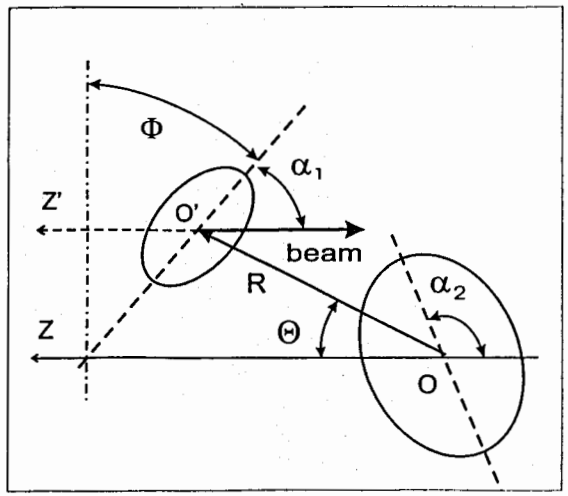

Fig.7. A sketch of the interaction between the deformed projectile-nucleus (the axial symmetry axis forms an angle α_1 with the beam) and the deformed target-nucleus (the axial symmetry axis forms an angle α_2 with the beam), with the impact parameter $b = R\cos\Theta$. The planes, in which the axial symmetry axes of nuclei lie, cross the Oz line and form an angle Φ

view, the evaluated fusion cross section (stars and open symbols) are overestimated. Consequently, since these fusion cross sections are close to our calculated capture cross sections, we assume that it is impossible to extract the fusion cross section from experimental data without any ambiguity because the compound nucleus stage is only one of the channels of reaction leading to the same reaction products, *i.e.* fusion is not the starting point of composite nuclear systems. Therefore, the method of extracting the fusion cross section from experimental data of the evaporation residues and/or light particle spectra without including the quasifission in entrance channel dynamics substantially leads one to identify the fusion and capture cross sections. These cross sections are significantly different for reactions with massive nuclei where quasifission is present.

Obviously, the calculated beam energy window for fusion can also be extended to higher energies if one includes the prethermalization emission of light charged particles in calculation. In fact, in this case the preequilibrium emission leads to the removal of a part of relative kinetic energy and to the increase of capture and fusion cross sections. The decrease of relative kinetic energy leads us to trap the dinuclear system into a potential pocket, increasing the energy window to larger energies. As affirmed by the authors of experiment [33], a significant evaporation of light charged particles came from the composite system with a very large effective deformation ($b/a \approx 2.8$). The latter, according to our approach, corresponds to a dinuclear system which evolves to fusion after capture in the initial stage. This means that indeed fusion is not such a very fast process as to neglect its relaxation time. The second reason is connected with the experimental condition. The authors could not exclude the detection of target-like fragments coming from a *deep inelastic process* mixed with evaporation residues due to similar masses.

5 Conclusions

The width of the energy window is analysed as a subject influenced by the entrance channel of reactions. It depends on the size of the potential pocket and dissipative properties of the formed dinuclear system which can be fused. The effect of the two peculiarities of the entrance channel is considered for the ^{19}F + ^{107}Ag and ^{28}Si + ^{98}Mo reactions leading to the same compound nucleus ^{126}Ba in the case of complete fusion. One of them is the pocket size of the nucleus-nucleus interaction potential which is different for these reactions. It defines the number of partial waves contributing to the capture and fusion cross sections, as well as the quasifission barrier for the dinuclear system formed after capture. It was clear that a more asymmetric system has a deeper potential pocket. The other peculiarity of the entrance channel is the different B_{fus} intrinsic fusion barrier which is defined by the position of initial values of the mass (charge) asymmetry in the potential energy surface. Again the more asymmetric ^{19}F + ^{107}Ag system is favorable to the fusion because it has a smaller value of the intrinsic fusion barrier in the mass (charge) asymmetry axis in the way to the fusion.

The calculations show that an energy dissipation takes place nearly continuously after the colliding nuclei have been touched, not immediately as was often assumed. The second important result is that if the above-mentioned barrier energy could not be enough dissipated, the capture does not take place like in the case of absence of pocket in the nucleus-nucleus potential. It seems to be one of the reasons why in the synthesis of the superheavy elements

the experimentalists observe a small window for the bombarding energy of projectile [3].It is revealed in the smallness of the excitation energy variance. This is an important point for reactions with massive nuclei where $U(R)$ usually has a small pocket. The comparison between calculated results and the available experimental data shows the role played by quasifission in reactions with massive nuclei and, at larger beam energies, also for the intermediate mass nuclei. The increase of the difference between the experimental evaporation residue and extracted fusion cross sections by the beam energy for the ^{40}Ar + ^{nat}Ag reaction is explained as an increasing effect of quasifission process. Therefore, if one does not include dynamical effects in the entrance channel in the analysis, the method to extract the fusion cross section from experimental data substantially leads one to identify the fusion and capture cross sections. Moreover, it is impossible to reach an agreement with the experimental data until the prethermalization emission of the light charged particles is taken into account.

Acknowledgements

The authors are grateful to Prof. V.V. Volkov, Drs. N.V. Antonenko, G.G. Adamian, and E.A. Cherepanov for the fruitful discussions. One of the authors (A.K.N) would like to express his gratitude for the warm hospitality during his stay at the Dipartimento di Fisica dell'Università di Messina, and also for the financial support from INFN, the Russian Foundation for Basic Research under grant No.97-02-16030 and the Uzbek State Foundation of the Scientific and Technical Committee No. 4/98.

Appendix A

The angles between the axial symmetry axis of the projectile- and target-nucleus and the beam direction are α_1 and α_2, respectively (Fig. 7). The spherical coordinate system O with the vector r, angles θ and ϕ is placed at the mass center of the target-nucleus and the Oz axis is directed opposite to beam. In this coordinate system, the direction of the vector $\mathbf{R}$ connecting the mass centers of interacting nuclei has angles Θ and Φ. The coordinate system is chosen thus that the planes, in which the axial symmetry axes of nuclei lie, cross the Oz line and form an angle Φ. For the head-on collisions $\Theta = 0$ and $\Phi = \phi$.

The nucleon distribution functions of interacting nuclei in integrand of (14) can be expressed using these variables in the same coordinate system O.

In the O system the axial symmetry axis of the target-nucleus is turned through an α_2 angle, so its nucleon distribution function is as follows:

$$\rho_2^{(0)}(\mathbf{r}) = \rho_0\Big\{1 + \exp\Big[\frac{r - R_0^{(2)}\left(1 + \beta_2^{(2)}Y_{20}(\cos\theta_2')\right)}{a}\Big]\Big\}^{-1}, \tag{27}$$

where ρ_0=0.17 fm^{-3},

$$\cos\theta_2' = \cos\theta\cos(\pi - \alpha_2) + \sin\theta\sin(\pi - \alpha_2)\cos\phi\,. \tag{28}$$

The mass center of the projectile-nucleus is shifted to the end of the vector $\mathbf{R}$ and its axial symmetry axis is turned through a $\pi - \alpha_1$ angle. According to the transformation formulae of

the parallel transfer of vectors the variables of the transferred system O' look as follows:

$$r'^2 = r^2 + R^2 - 2rR\cos(\omega_{12}), \tag{29}$$

$$\cos(\omega_{12}) = \cos\theta\cos\Theta + \sin\theta\sin\Theta\cos(\phi - \Phi), \tag{30}$$

$$\cos\theta_1' = \frac{(r\cos\theta - R\cos\Theta)}{r'},$$

$$\cos\phi_1' = (1 + \tan^2\phi_1')^{-1/2}, \tag{31}$$

$$\tan\phi_1' = \frac{r\sin\phi\sin\theta - R\sin\Theta\sin\Phi}{r\cos\phi\sin\theta - R\sin\Theta\cos\Phi}. \tag{32}$$

In the coordinate system O', the deviation of the axial symmetry axis of projectile-nuclei relative to the $O'z'$ axis is determined by the angle

$$\cos\theta_1'' = \cos\theta_1'\cos(\pi - \alpha_1) + \sin\theta_1'\cos\phi_1'. \tag{33}$$

Now the nucleon distribution function of the projectile-nucleus looks like

$$\rho_1^{(0)}(\mathbf{r}, R) = \rho_0\Big\{1 + \exp\Big[\frac{r' - R_0^{(1)}\left(1 + \beta_2^{(1)}Y_{20}(\cos\theta_1')\right)}{a}\Big]\Big\}^{-1}. \tag{34}$$

The nuclear part of the nucleus-nucleus potential was calculated by the folding procedure of the effective nucleon-nucleon forces by Migdal [19] with the nucleon distribution functions (27) and (34) of interacting nuclei:

$$V_{nucl}(\mathbf{R}) = \int \rho_1^{(0)}(\mathbf{r}, \mathbf{R}) f_{eff}[\rho(\mathbf{r})]\rho_2^{(0)}(\mathbf{r})d^3\mathbf{r}. \tag{35}$$

Appendix B

The value of τ_i is calculated using the results of the theory of quantum liquids [27] and the effective nucleon-nucleon forces from [19]:

$$\frac{1}{\tau_i^{(\alpha)}} = \frac{\sqrt{2}\pi}{32\hbar\varepsilon_{F_K}^{(\alpha)}}\Big[(f_K - g)^2 + \frac{1}{2}(f_K + g)^2\Big]\Big[\left(\pi\Theta_K\right)^2 + \left(\tilde{\varepsilon}_i - \lambda_K^{(\alpha)}\right)^2\Big] \times \Big[1 + \exp\Big(\frac{\lambda_K^{(\alpha)} - \tilde{\varepsilon}_i}{\Theta_K}\Big)\Big]^{-1}, \tag{36}$$

where

$$\Theta_K(t) = 3.46\sqrt{\frac{E_K^*(t)}{< A_K(t) >}}$$

is the effective temperature determined by the amount of the intrinsic excitation energy $E_K^* = E_K^{*(Z)} + E_K^{*(N)}$, and by the mass number $< A_K(t) >$ (with $< A_K(t) >=< Z_K(t) > + < N_K(t) >$). In addition, $\lambda_K^{(\alpha)}(t)$ and $E_K^{*(\alpha)}(t)$ are the chemical potential and intrinsic excitation energies for the proton ($\alpha = Z$) and neutron ($\alpha = N$) subsystems of the nucleus $K(K = 1(\text{projectile}), 2(\text{target}))$, respectively. Furthermore, the finite size of nuclei and the available difference between the numbers of neutrons and protons need to use the following expressions for the Fermi energies [19]:

$$\varepsilon_{F_K}^{(Z)} = \varepsilon_F\Big[1 - \frac{2}{3}(1 + 2f_K')\frac{< N_K > - < Z_K >}{< A_K >}\Big],$$

$$\varepsilon_{F_K}^{(N)} = \varepsilon_F\Big[1 + \frac{2}{3}(1 + 2f_K')\frac{< N_K > - < Z_K >}{< A_K >}\Big], \tag{37}$$

where ϵ_F=37 MeV,

$$f_K = f_{in} - \frac{2}{< A_K >^{1/3}}(f_{in} - f_{ex}),$$
$$f'_K = f'_{in} - \frac{2}{< A_K >^{1/3}}(f'_{in} - f'_{ex}) \qquad (38)$$

and f_{in}=0.09, f'_{in}=0.42, f_{ex}=-2.59, f'_{ex}=0.54, g=0.7 are the constants of the effective nucleon-nucleon interaction.

References

1. W. J. Swiatecki, Phys. Scr. 24 (1981) 113.
2. S. Hofmann, Z. Phys. A350 (1995) 281.
3. S. Hofmann, GSI-Preprint-97-57, Darmstadt, 1997.
4. H. Gäggeler, T. Sikkeland, G. Wirth, W. Bruchle, W. Bogl, G. Franz, G. Herrmann, J.V. Kratz, M. Schaedel, K. Summerer, and W. Weber, Z. Phys. A316 (1984) 291.
5. G.V. Ravi Prasad and V.S. Ramamurthy, Phys. Rev. C54 (1996) 815.
6. G.V. Ravi Prasad, V.S. Ramamurthy, and R.T. Yadav, Phys. Rev. C51 (1995) 2833.
7. P. Fröbrich, Phys. Rep. 116 (1984) 337.
8. N.V. Antonenko, E.A. Cherepanov, A.K. Nasirov, V.P. Permjakov and V.V. Volkov, Phys. Lett. B319 (1993) 425; Phys. Rev. C51 (1995) 2635.
9. E.A. Cherepanov, V.V. Volkov, N.V. Antonenko, V.P. Permjakov, and A.K. Nasirov, Nucl. Phys. A583 (1995) 165c.
10. E.A.Cherepanov, G.G. Adamian, N.V.Antonenko, A.K.Nasirov, V.V. Volkov, Proc. Int. Conf. on Large-Scale Collective Motion of Atomic Nuclei (Brolo, Italy 1996), ed. G. Giardina, G. Fazio, and M. Lattuda (World Scientific, Singapore, 1997) p. 69.
11. R.V. Jolos, A.I. Muminov, A.K. Nasirov, JINR Preprint E4-97-302, Dubna, 1997; to be published in Europ. Phys. Journal A.
12. G.G. Adamian, N.V. Antonenko, W. Scheid, V.V. Volkov, Nucl. Phys. A633 (1998) 409.
13. G.G. Adamian, R.V. Jolos, A.I. Muminov, and A.K. Nasirov, Phys. Rev. C53 (1996) 871.
14. G.G. Adamian, R.V. Jolos, A.I. Muminov, and A.K. Nasirov, Phys. Rev. C56 (1997) 373.
15. G.G. Adamian, R.V. Jolos, and A.K. Nasirov, Z. Phys. A347 (1994) 203.
16. A. H. Wapstra and G. Audi, Nucl. Phys., A432 (1985) 1.
17. P. Möller and J.R. Nix, Preprint LA-UR-86-3983, Los Alamos National Laboratory, 1986.
18. C.Y. Wong, Phys. Rev. Lett. 31 (1973) 766.
19. A.B. Migdal, Theory of the Finite Fermi-Systems and Properties of Atomic Nuclei, Moscow, Nauka, 1983 (in Russian).
20. N. Rowley, G.R. Satchler and P.H. Stelson, Phys. Lett. B254 (1991) 25.

21. J.X. Wei, J.R. Leigh, D.J. Hinde, J.O. Newton, R.C. Lemmon, S. Elfström, J.X. Chen, and N. Rowley, Phys. Rev. Lett. 67 (1991) 3368.
22. N. Rowley, Nucl. Phys. A538 (1992) 205c.
23. J.R. Leigh, et al., Phys. Rev. C47 (1991) R437.
24. S. Raman, C.H. Malarkey, W.T. Milner, C.W. Nestor, Jr., and P.H. Stelson, Atomic Data and Nuclear Data Tables 36 (1987) 1.
25. S. Hofmann, private communication.
26. H.S. Köhler, Nucl. Phys. A343 (1980) 315; A378 (1982) 181.
27. D. Pines and P. Noziéres, Theory of Quantum Liquids, Benjamin, New York, 1966.
28. G.G. Adamian, R.V. Jolos, and A.K. Nasirov, Sov. J. Nucl. Phys. **55** (1992) 660.
29. G.G. Adamian, N.V. Antonenko, R.V. Jolos, and A.K. Nasirov, Nucl. Phys. **A551** (1993) 321.
30. G. G. Adamian, A. K. Nasirov, N. V. Antonenko, and R.V. Jolos, Phys. Part. Nucl. 25 (1994) 583.
31. W.U. Schröder, J.R. Birkelund, J.R. Huizenga, K.L. Wolf, and V.E. Viola Jr., Phys. Rep. 45 (1987) 301.
32. H.C. Britt, B.H. Erkilla, R.H. Stokes, H.H. Gutbrod, F. Plasil, R.L. Ferguson and M. Blann, Phys. Rev. C13 (1976) 1483.
33. Roy Lacey, N.N. Ajitand, John M. Alexander, D.M. de Castro Rizzo, G.F. Peaslee, L.C. Vaz, Morton Kaplan, M. Kildir, G. La Rana, D.J. Moses, and W.E. Parker, D. Logan, M.S. Zisman, P. DeYoung, and L. Kowalski, Phys. Rev. C37 (1988) 2540.
34. H.H. Gutbrod, F. Plasil, H.C. Britt, B.H. Erkilla, R.H. Stokes, and M. Blann, in Proc. of the III Int. Atomic Energy Symposium on the Physics and Chemistry of Fission, Rochester, 1973; Int. Atomic Energy Agency, Vienna, Austria, 1974, Vol.II, p. 309.
35. C. Cerruti, D. Guinet, S. Chiodelli, A. Demeyer, K. Zaïd, S. Leray, P. Lhenoret, C. Mazur, C. Ngô, M. Ribrag, A. Lleres, Nucl. Phys. A453 (1986) 175.
36. B. Borderie, M.F. Rivet, C. Cabot, D. Fabris, D. Gardes, H. Gauvin, F. Hanappe, and J. Peter, Z. Phys. A316 (1984) 243.
37. M.T. Magda, T. Ethvignot, A. Elmaani, J.M. Alexander, P. Désesquelles, H. Elhage, A. Giorni, D. Heuer, S. Kox, A. Lleres, F. Merchez, C. Morand, D. Rebreyend, P. Stassi, J.B. Viano, F. Benrachi, B. Chambon, B. Cheynis, D. Drain, and C. Pastor, Phys. Rev. C45 (1992) 1209.

Received by Publishing Department
on October 5, 1998.

Джиардина Дж. и др. E4-98-279

Конкуренция между квазиделением и слиянием после захвата в столкновениях тяжелых ионов

Исследована зависимость разницы между полным слиянием и захватом от входного канала в рамках комбинированной динамической и статистической модели. Рассчитаны функции возбуждения составного ядра ^{126}Ba, образуемого в реакциях $^{19}F + ^{107}Ag$ и $^{28}Si + ^{98}Mo$. Установлены границы окна слияния E_{min} и E_{max} для энергии пучка. Проведено сравнение теоретических результатов с сечениями слияния, извлеченными из экспериментальных сечений образования ядра отдачи в реакции $^{40}Ar + ^{nat}Ag$. Отмечена важность роли конкуренции квазиделения с полным слиянием и энергетического окна для захвата при интерпретации событий, наблюдаемых в эксперименте.

Работа выполнена в Лаборатории теоретической физики им. Н.Н.Боголюбова ОИЯИ.

Препринт Объединенного института ядерных исследований. Дубна, 1998

Giardina G. et al. E4-98-279

Competition between Quasifission and Fusion after Capture in Heavy-Ion Collisions

A dependence of the difference between the complete fusion and capture processes is studied as a function of the entrance channel in the framework of the combined dynamical and statistical model. The excitation functions for the compound nucleus ^{126}Ba formed in the $^{19}F + ^{107}Ag$ and $^{28}Si + ^{98}Mo$ reactions were calculated. Borders of a beam energy window for the fusion cross section, E_{min} and E_{max}, were established. The experimental data on evaporation residues and extracted from them fusion cross sections and the theoretical results for the $^{40}Ar + ^{nat}Ag$ reaction were compared. The importance of competition between quasifission and complete fusion and of the beam energy window for the capture for interpretation of the observed experimental data is discussed.

The investigation has been performed at the Bogoliubov Laboratory of Theoretical Physics, JINR.

Preprint of the Joint Institute for Nuclear Research. Dubna, 1998